JOURNAL OF SOLID STATE CHEMISTRY 51, 293–299 (1984)

Ionic Conductivity of Oxides with General Formula $Li_xLn_{1/3}Nb_{1-x}Ti_xO_3$ (*Ln* = La, Nd)

L. LATIE, G. VILLENEUVE, D. CONTE, AND G. LE FLEM

Laboratoire de Chimie du Solide du CNRS, Ecole Nationale Supérieure de Chimie et de Physique de Bordeaux, Université de Bordeaux I, 351, cours de la Libération, 33405 Talence Cedex, France

Received June 8, 1983; in revised form August 26, 1983

Ionic conductivity of phases with general formula $Li_xLn_{1/3}Nb_{1-x}Ti_xO_3$ (*Ln* = La, Nd) has been determined for materials with a small value of x, i.e., in composition range with a $Ln_{1/3}NbO_3$ perovskite related structure. The possible influence on the transport properties of the 2D character of the vacancy sublattice has been investigated by a NMR study on $Li_{0.05}Nb_{0.95}Ti_{0.05}O_3$.

Materials with general formulation $Ln_{1/3}NbO_3$ (*Ln* = La, Ce, Pr, Nd) have been isolated by Dyer and White (*1*). Their structure has been described by Iyer and Smith (*2*). It is related to the perovskite type. Niobium occupies oxygen octahedra sharing common corners in the three space directions. The rare earths are in the 12-coordinated sites with an ordered distribution: parallel to the c axis one [12] site is entirely empty and one is statistically occupied by 2/3 *Ln* (Fig. 1). Hence there are in the (001) planes two alternating vacancy sublattices which we may call respectively □ and □′. The introduction of ions of various size and charge may be expected in those vacancies, as far as a charge compensation results from partial substitution of Nb^{5+} by less charged ions Ti^{4+}, for instance (*3*). In the eventuality the inserted ion is monovalent, ion conductivity can be expected, with transport properties eventually related to the 2D character of the □ sublattice (Fig. 1).

We describe successively here:

—the crystal chemical evolution of the $Li_xLn_{1/3}Nb_{1-x}Ti_xO_3$ (*Ln* = La, Nd) for small values of x, i.e., with a composition close to $Ln_{1/3}NbO_3$,

—the composition dependence of the ionic conductivity

—a NMR study of the conduction mechanism of Li^+ for the best ionic conductor obtained with composition $Li_{0.05}La_{1/3}Nb_{0.95}Ti_{0.05}O_3$.

I. Experimental Procedure and Crystal Chemical Evolution

Different compositions have been obtained from a mixture of La_2O_3 or Nd_2O_3, TiO_2, Nb_2O_5, and Li_2CO_3 in the proportions given by the stoichiometric reaction

$$\frac{x}{2}\,Li_2CO_3 + \frac{1}{6}\,Ln_2O_3 + \frac{1-x}{2}\,Nb_2O_5 + xTiO_2 \rightarrow Li_xLn_{1/3}Nb_{1-x}Ti_xO_3 + \frac{x}{2}\,CO_2\uparrow$$

0022-4596/84 $3.00

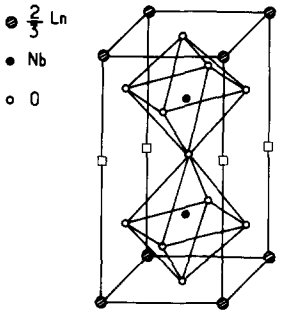

FIG. 1. Crystal structure of $Ln_{1/3}NbO_3$.

The reaction temperature is about 1200°C. The lanthanum compounds are white, the neodynium compounds violet-red.

Table I gives the crystallographic data for some of the materials obtained. The lithium insertion rate is low; it is higher for the lanthanum compounds ($x < 0.10$) than for the neodynium one ($x < 0.07$).

II. Ionic Conductivity Determinations

The samples are cylindrical pellets ($\phi = 8$ mm) initially sintered at 1200°C with a compactness up to 90%.

Conductivity measurements have been carried out from 20 to 400°C using ionically blocking electrodes and an ac technique over a wide frequency range.

In that temperature domain the thermal variation of the conductivity follows an Arrhénius law, $\log \sigma = Ae - \Delta E/kT$, where ΔE is the activation energy related to the conduction mechanism.

Figure 2 gives the results obtained for the richest lithium compounds in both systems. They are compared with those relative to $Na_{0.05}Nd_{1/3}Nb_{0.95}Ti_{0.05}O_3$ (*3*).

It may be observed that:

—in each phase the conductivity increases with the Li^+ content. It results from the increasing number of carriers;
—higher conductivity is obtained with lithium than with sodium for homologous materials;
—the conductivity is higher for the lanthanum compound than for the neodynium one.

The two last results show very clearly the important influence of the steric parameters

TABLE I

CRYSTALLOGRAPHIC DATA RELATIVE TO $Li_xLn_{1/3}Nb_{1-x}Ti_xO_3$ PHASES

	Cell parameters ± 0.002 (Å)	Atomic coordinates				$d_{obs.}$	$d_{calc.}$
			x/a	*y/b*	*z/c*		
$La_{1/3}NbO_3$	$a = 3.910$	La	0	0	0		
		Nb	0.5	0.5	0.26		
	$b = 3.920$	O_1	0	0.5	0.23	5.11	5.13
		O_2	0.505	0.51	0		
	$c = 7.910$	O_3	0.505	0.51	0.5		
$La_{0.10}Li_{0.33}Nb_{0.90}Ti_{0.13}O$	$a = 3.915$						
	$b = 3.920$					5.09	5.08
	$c = 7.920$						
$Nd_{1/3}NbO_3$	$a = 3.910$						
(2)	$b = 3.930$					5.25	5.26
	$c = 7.780$						
$Li_{0.07}Nd_{0.33}Nb_{0.93}Ti_{0.07}O_3$	$a = 3.880$						
	$b = 3.882$					5.20	5.31
	$c = 7.780$						

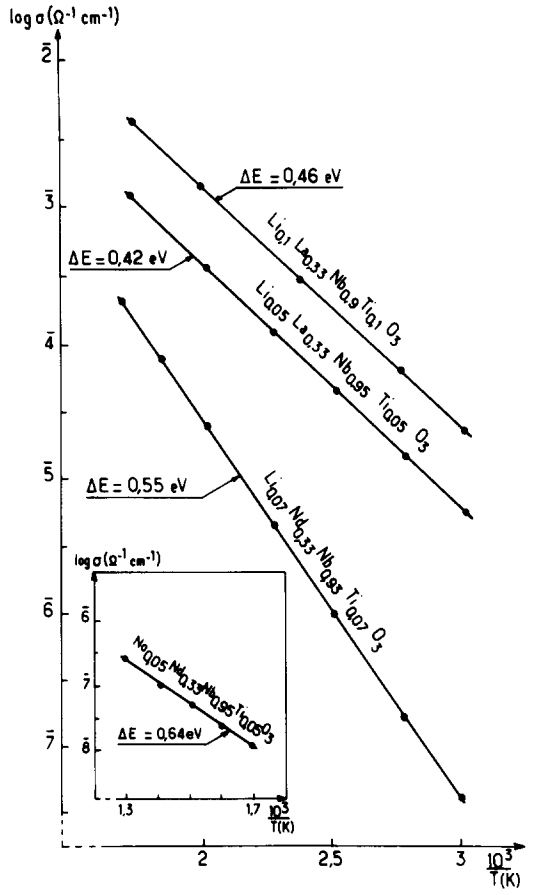

FIG. 2. Ionic conductivity of $Li_xLn_{1/3}Nb_{1-x}Ti_xO_3$ phases.

on the electrical properties of the oxides, all the more as the activation energy decreases when sodium is replaced by lithium and neodynium by lanthanum. This conclusion led us to investigate the conduction mechanism.

From the atomic positions of $La_{1/3}NbO_3$ (*2*) (Table I) it is possible to calculate the area of the various bottlenecks existing inside the □ or inside the □′ sublattices or between them (Fig. 1). Those areas are, respectively, 17, 14, and 15.3 Å^2. By considering only the steric factor, the motion appears to be the easiest within the previously empty −□ sublattice.

On the other hand the respective cationic and anionic distributions show that the charge carried by oxygen atoms increases when we consider successively O_1, O_2, and O_3 as the number of bonds of the oxygen atoms decreases. Therefore, from the electrostatic point of view one could expect that lithium diffusion must become progressively easier within □, between □ and □′, and within □′.

It results that steric and electrostatic influences are in competition.

Since two-thirds of the rare earth positions are occupied the lithium motion must have essentially a 2D character within □, but possible diffusion via □′ cannot be excluded. To check such an hypothesis a NMR investigation on ^7Li in $Li_{0.05}La_{1/3}Nb_{0.95}Ti_{0.05}O_3$ has been carried out.

III. NMR Study of $Li_{0.05}La_{1/3}Nb_{0.95}Ti_{0.05}O_3$

III-1. Experimental Conditions

The absorption spectra have been obtained at 21 MHz with a Bruker SWL 100 continuous wave (cw) spectrometer using the cross-coil technique. The magnetic field was produced by a Drusch magnet and sweeping was monitored with a Hall probe.

Spin–lattice relaxation times have been obtained with a Bruker SXP 3-100 and 19.00, 25.00, and 34.97 MHz using the π–τ–$\pi/2$ classical sequence. The magnetic field provided by a Brucker magnet was stabilized by a proton NMR probe or a Hall probe. To improve the signal to noise ratio the sequences were accumulated 100 times by coupling the spectrometer with a HP 9825 computer.

The thermal variation between 150 and 450 K has been determined by blowing cooled or heated dry nitrogen, on the sample. The temperature was stabilized with an accuracy of ±1 K during each measurement.

III-2. Results Obtained

(a) Linewidth. Figure 3 shows three ab-

sorption spectra characterizing the thermal behaviour of the resonance lines.

Only one Gaussian line appears at low temperature ($T < 170$ K) as indicated by Fig. 3a where the peak-to-peak width is $\Delta H = 3.2$ G. Such a "rigid lattice" behavior results from the low mobility of the Li^+ ions, whose jump frequency is lower than the dipolar line width $\nu_j \leq 5 \times 10^3$ sec^{-1}.

At rising temperature the Li^+ motion becomes faster, leading to narrowing of the previous broad line. Nevertheless this line is still a very wide one, as shown in Fig. 3b, emphasizing that some Li^+ ions have not reached the critical jump frequency. The intensity of the broad line decreases up to 300 K and at higher temperature only a narrow line with Lorentzian shape is observed (Fig. 3c).

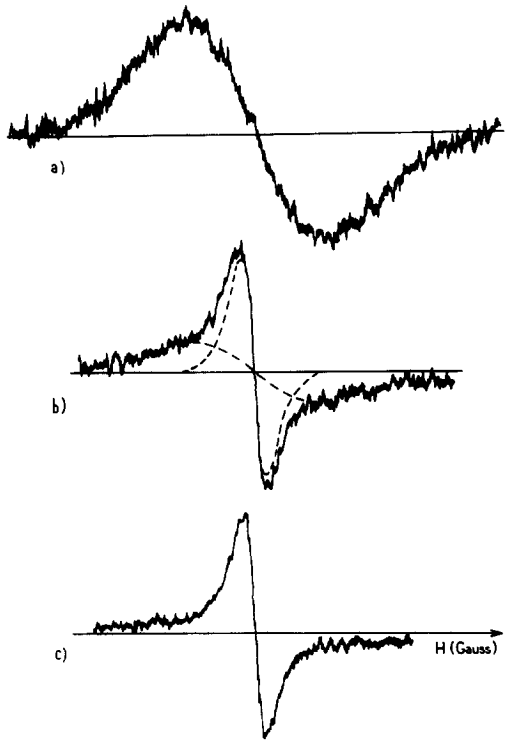

FIG. 3. First derivative of the ^7Li absorption line in $Li_{0.05}La_{1/3}Nb_{0.95}Ti_{0.05}O_3$ at three temperatures: (a) 140 K. (b) 245 K. The dashed lines show the deconvolution of the spectrum into two lines. (c) 450 K.

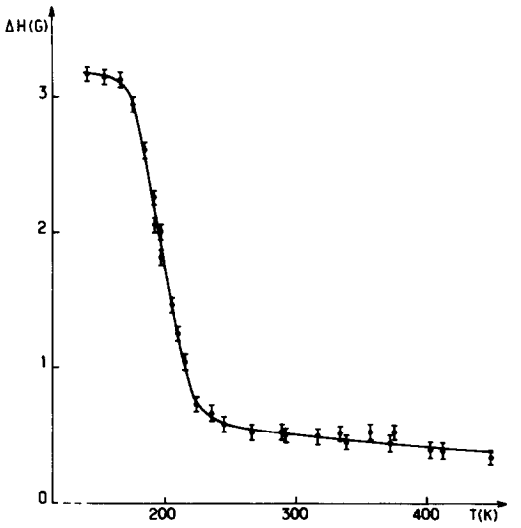

FIG. 4. Temperature dependence of the ^7Li linewidth in $Li_{0.05}La_{1/3}Nb_{0.95}O_3$.

Figure 4 shows the thermal evolution of the peak-to-peak linewidth relative to the more mobile Li^+ ions. In the narrowing regime the linewidth depends on the jump frequency ν_j following a relation given by Whittingham *et al.* (*4*):

$$\nu_j = \alpha \frac{\gamma}{2\pi} \frac{\Delta H - \Delta H_r}{\tan \frac{\pi}{2} \left(\frac{\Delta H - \Delta H_r}{\Delta H_0 - \Delta H_r}\right)^2}$$

where ΔH_0 is the linewidth corresponding to the rigid lattice behavior, ΔH_r the residual width resulting from magnetic field inhomogeneities in the sample, ΔH the experimental line width at given temperature, and γ the gyromagnetic ratio of the resonant nucleus. α is a coefficient varying from 1 to 10 according to the jump mechanism. Clearly it affects only the preexponential factor.

The variation of ν_j/α vs reciprocal temperature is given in Fig. 5. The jump frequency is thermally activated according to an Arrhenius law

$$\nu_j/\alpha = 3.6 \times 10^8 \exp(-0.18 \text{ eV}/kT).$$

The observed activation energy is much

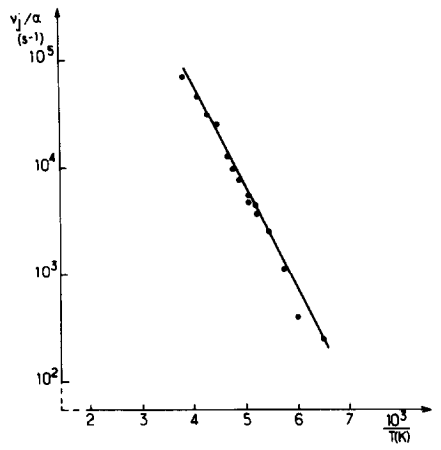

FIG. 5. Li^+ jump frequency vs reciprocal temperature obtained from linewidth analysis.

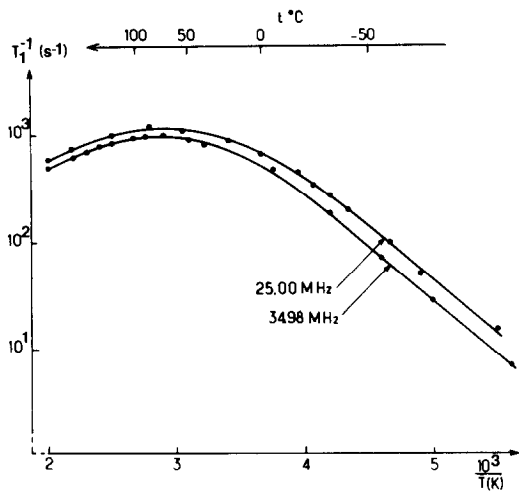

FIG. 6. Spin–lattice relaxation rate vs reciprocal temperature at 25.00 and 34.97 MHz.

lower than the value obtained from the thermal behavior of ionic conductivity (E_a = 0.42 eV). Such a discrepancy is often observed since NMR is sensitive to the local motions which involve lower energy barriers than diffusion processes.

(b) Spin–lattice relaxation. The evolution of spin–lattice relaxation T_1^{-1} with reciprocal temperature is given in Fig. 6 for two frequencies, 25.00 and 34.97 MHz. Both curves show a maximum at about 350 K.

Although the continuous wave spectra give no evidence of a quadrupolar effect, the spin–lattice relaxation can be due either to the fluctuations of the dipolar interactions or to the fluctuations of the electric field gradient seen by the nuclei. In both cases, if the simple Blombergen–Purcell–Pound (BPP) model (*5*) is used, the spin–lattice relaxation is

$$T_1^{-1} = C\left(\frac{\tau_c}{1 + \omega_0^2\tau_c^2} + \frac{4\tau_c}{1 + 4\omega_0^2\tau_c^2}\right)$$

where C is a constant depending on the interactions responsible for the relaxation, ω_0 the Larmor frequency, and τ_c the correlation time of the motion.

The BPP model predicts a relaxation maximum at $\omega_0\tau_c = 0.62$. Consequently it is possible from the experimental maximum of T_1^{-1} to determine the thermal evolution of the jump frequency (Fig. 7):

$$\nu_j = 8.5 \times 10^{10} \exp(-0.165 \text{ eV}/kT) \quad \text{at 34.97 MHz}$$

$$\nu_j = 5.5 \times 10^{10} \exp(-0.160 \text{ eV}/kT) \quad \text{at 25.00 MHz.}$$

Therefore a good agreement is revealed

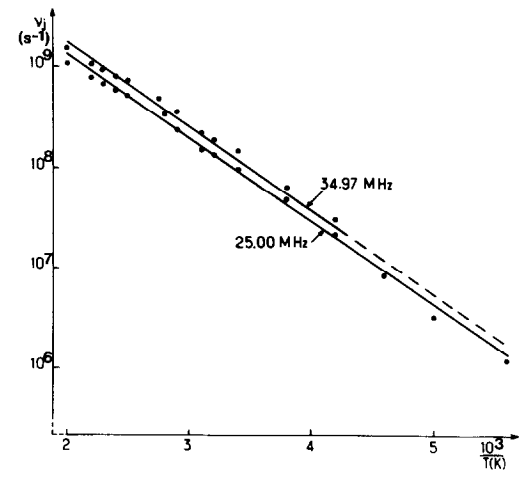

FIG. 7. Li^+ jump frequency vs reciprocal temperature at 25.00 and 34.97 MHz obtained from BPP analysis of the spin–lattice relaxation rate.

between the activation energy deduced from the linewidth measurements and that obtained from the spin–lattice relaxation.

The large discrepancy observed for the preexponential factor is due in particular to the value of α which may vary by an order of magnitude in the expression of ν_j/α obtained from the linewidth.

IV. Discussion

In Section II three possible mechanisms of Li^+ jumps based on the crystal structure were considered:

$$\square \rightarrow \square; \qquad \square' \rightarrow \square'; \qquad \square \rightarrow \square'.$$

The two first give rise to a 2D conduction whereas the third one involves a 3D mechanism. We shall examine those hypotheses on hand of the results obtained from the relaxation study which are sensitive to the dimensionality of the ion motion in consideration of, successively, the preexponential factor and the frequency dependence of T_1^{-1} in the low temperature regime.

(i) The preexponential factor obtained from a (isotropic) BPP model and corresponding to the characteristic vibration frequencies of the mobile species (typically 10^{12}–10^{13} sec^{-1}) is significantly higher than the value observed here (0.8×10^{11} sec^{-1}). Such a discrepancy is often detected for low dimensional conductors: Walstedt *et al.* *al.* (*6*), for instance, studying the ^{23}Na spin–lattice relaxation in the 2D β-alumina (conductor), obtained a preexponential factor of 2×10^{11} sec^{-1}, which is close to our own value.

(ii) To specify the frequency dependence of T_1^{-1}, measurements have been carried out at 19.80 MHz in the low temperature regime of the BPP model. Due to low concentration of Li^+ ions, the signal to noise ratio was too low to allow an accurate determination of the relaxation rates at lower frequencies. The BPP model predicts at low

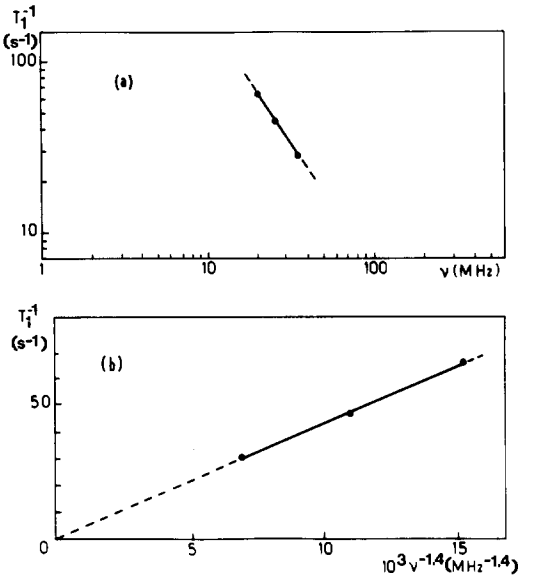

FIG. 8. (a) Log–log plot of spin–lattice relaxation rate vs frequency at 200 K. (b) Spin–lattice relaxation rate vs $\nu_0^{-1.4}$.

temperature, when $\omega_0^2\tau_c^2 \gg 1$, at T_1^{-1} variation proportional to ω_0^{-2} (or ν_0^{-2} with $\nu_0 = \omega_0/2\pi$). Figure 6 shows clearly that we do not observe such a behavior. A log–log plot given in Fig. 8a leads to a frequency variation of T_1^{-1} proportional to $\nu_0^{-1.4}$. This relation is confirmed in Fig. 8b: one can see that the T_1^{-1} vs $\nu_0^{-1.4}$ variation corresponds to a straight line going through the origin. A deviation from a ω_0^{-2} is frequently attributed to low dimensionality of the ionic motion: for instance, a $\omega_0^{-1.2}$ variation of T_1^{-1} has been found in β-alumina (*6*), but a log ω_0 variation is observed in TaS_2, NH_3 (*7*).

In fact other effects could play a part in the anomalies of the relaxation rate: the statistical distribution of Nb and Ti on one hand, and of La and $\square'$ vacancies on the other, give rise to a statistical distribution of the energy barriers between the $\square$ and $\square'$ planes. Walstedt *et al.* (*6*) proposed a phenomenological model based on a statistical distribution of the barriers around a mean

value E_a. This model leads to discrepancies from the BPP model similar to those resulting from a low dimensionality hypothesis.

In conclusion, structural and NMR considerations seem to give evidence of essentially bidimensional Li^+ jumps in the almost empty □ planes of the lattice. But some motions through the □′ vacancies are not excluded with an energy barrier distribution between □ or □′ vacancies. The lack of structural data for the phases investigated prevented us from locating the Li^+ ions in a give type of vacancies (or in both).

References

1. A. J. DYER AND E. A. D. WHITE, *Trans. Brit. Ceram. Soc.* **63**(6), 301 (1964).
2. P. N. IYER AND A. J. SMITH, *Acta Crystallogr.* **23,** 470 (1967).
3. D. CONTE, Thèse de 3ème cycle, Université de Bordeaux I (1983).
4. M. S. WHITTINGHAM, P. S. CONNEL, AND J. HUGGINS, *J. Solid State Chem.* **5,** 321 (1972).
5. N. BLOMBERGEN, E. M. PURCELL, AND R. V. POUND, *Phys. Rev.* **73,** 679 (1948).
6. R. E. WALSTEDT, R. DUPREE, J. P. REMEIKA, AND A. RODRIGUEZ, *Phys. Rev. B* **15,** 3442 (1977).
7. B. G. SILBERNAGEL AND F. R. GAMBLE, *Phys. Rev. Lett.* **32,** 1436 (1974).